Neutron scattering from ^{208}Pb at 30.4 and 40.0 MeV and isospin dependence of the nucleon optical potential

R. P. DeVito,[1,*] Dao T. Khoa,[2,†] Sam M. Austin,[1,3,‡] U. E. P. Berg,[1,§] and Bui Minh Loc[1,‖]

[1]*National Superconducting Cyclotron Laboratory and Department of Physics and Astronomy, Michigan State University, East Lansing, Michigan 48824-1321, USA*

[2]*Institute for Nuclear Science and Technique, VAEC, 179 Hoang Quoc Viet, Hanoi, Vietnam*

[3]*Joint Institute for Nuclear Astrophysics, Michigan State University, East Lansing, Michigan 48824-1321, USA*

(Received 10 January 2012; revised manuscript received 31 January 2012; published 27 February 2012)

Background: Analysis of data involving nuclei far from stability often requires the optical potential (OP) for neutron scattering. Because neutron data are seldom available, whereas proton scattering data are more abundant, it is useful to have estimates of the difference of the neutron and proton optical potentials. This information is contained in the isospin dependence of the nucleon OP. Here we attempt to provide it for the nucleon-^{208}Pb system.

Purpose: The goal of this paper is to obtain accurate $n + {}^{208}$Pb scattering data and use it, together with existing $p + {}^{208}$Pb and ^{208}Pb$(p,n)^{208}$Bi$^*_{\rm IAS}$ data, to obtain an accurate estimate of the isospin dependence of the nucleon OP at energies in the 30–60-MeV range.

Method: Cross sections for $n + {}^{208}$Pb scattering were measured at 30.4 and 40.0 MeV, with a typical relative (normalization) accuracy of 2–4% (3%). An angular range of 15° to 130° was covered using the beam-swinger time-of-flight system at Michigan State University. These data were analyzed by a consistent optical-model study of the neutron data and of elastic $p + {}^{208}$Pb scattering at 45 and 54 MeV. These results were combined with a coupled-channel analysis of the ^{208}Pb(p,n) reaction at 45 MeV, exciting the 0^+ isobaric analog state (IAS) in ^{208}Bi.

Results: The new data and analysis give an accurate estimate of the isospin impurity of the nucleon-^{208}Pb OP at 30.4 MeV caused by the Coulomb correction to the proton OP. The corrections to the real proton OP given by the CH89 global systematics were found to be only a few percent, whereas for the imaginary potential it was greater than 20% at the nuclear surface. On the basis of the analysis of the measured elastic $n + {}^{208}$Pb data at 40 MeV, a Coulomb correction of similar strength and shape was also predicted for the $p + {}^{208}$Pb OP at energies around 54 MeV.

Conclusions: Accurate neutron scattering data can be used in combination with proton scattering data and (p, n) charge exchange data leading to the IAS to obtain reliable estimates of the isospin impurity of the nucleon OP.

DOI: 10.1103/PhysRevC.85.024619 PACS number(s): 25.40.Dn, 24.10.Ht, 24.10.Eq

I. INTRODUCTION

At energies below 100 MeV, the attraction between a neutron and a proton is stronger than that between two protons or two neutrons. Consequently, the average interaction of a proton with an $N > Z$ nucleus is stronger than that of a neutron. In other words, the nuclear interaction between an incident nucleon and a target with nonzero isospin has an isospin-dependent part. For the nuclear part of the nucleon-nucleus optical potential (OP), the isospin-dependent term is, in the Lane form [1],

$$U_N = U_0 + 4U_1 \frac{\boldsymbol{t} \cdot \boldsymbol{T}}{A}, \tag{1}$$

where $\boldsymbol{t}$ is the isospin of the incident nucleon and $\boldsymbol{T}$ is that of the target A. The second term of Eq. (1), known as the Lane potential, contributes to both the elastic (p,p) and (n,n) scattering as well as to the charge-exchange (p,n) reaction [2,3]. A knowledge of U_1 is of fundamental interest for studies of nuclear phenomena in which neutrons and protons participate differently (isovector modes). Many previous estimates of U_1 (see, for example, Refs. [4–6]) involved a comparison of the nucleon OP from a range of nuclei with different values of the asymmetry parameter $\varepsilon = (N - Z)/A$ or the distorted-wave Born approximation (DWBA) analysis of (p,n) reactions exciting the isobaric analog state (IAS). However, these approaches are subject to serious uncertainties. For example, in the comparison of elastic nucleon scattering from different nuclei one must make assumptions [4] about the variation of nuclear geometry with A and ε. Moreover, the contribution of the Lane potential U_1 to the elastic nucleon scattering cross section is relatively small [7,8]. In contrast, U_1 entirely determines the (Fermi-type) $\Delta J^\pi = 0^+$ transition strength of the (p,n) reaction exciting the IAS; this reaction is, therefore, a sensitive probe of the isospin dependence of the proton-nucleus OP [9]. However, for (p,n) reactions, a change in ReU_1 can be approximately compensated by a change in

*Present address: MSU Technologies, 325 East Grand River, Suite 350, East Lansing, Michigan 48823, USA.

†khoa@vaec.gov.vn

‡austin@nscl.msu.edu

§Present address: Berg Consult, D-73734 Esslingen, Germany.

‖Present address: University of Pedagogy, Ho Chi Minh City, Vietnam.

$\mathrm{Im}U_1$ [10], and the determination of U_1 remains ambiguous without additional information or constraints.

It is in principle possible to avoid these uncertainties by extracting U_1 from a consistent study of the elastic proton and neutron scattering and the charge-exchange (p,n) reaction on the same target nucleus, at the same energy. We recall here briefly the consistent isospin coupling scheme [3] for the elastic nucleon-nucleus scattering and charge-exchange (p,n) reaction exciting IAS. For the isospin projections $T_z = (N-Z)/2$ of the target nucleus A and $\tilde{T}_z = T_z - 1$ of the *isobaric analog nucleus* $\tilde{A}$, and denoting the neutron- and proton-scattering states by $|nA\rangle$ and $|pA\rangle$, respectively, the neutron and proton optical potentials are given by the diagonal matrix elements of potential (1):

$$U_p = \langle pA|U_N|pA\rangle = U_0 - \frac{2}{A}T_z U_1 = U_0 - \varepsilon U_1, \quad (2)$$

$$U_n = \langle nA|U_N|nA\rangle = U_0 + \frac{2}{A}T_z U_1 = U_0 + \varepsilon U_1. \quad (3)$$

Similarly, the transition matrix element or (p,n) form factor for the charge-exchange $A(p,n)\tilde{A}_{\mathrm{IAS}}$ reaction exciting IAS is

$$F_{pn} = \langle n\tilde{A}|4U_1\frac{\boldsymbol{t}\cdot\boldsymbol{T}}{A}|pA\rangle = \frac{2}{A}\sqrt{2T_z}U_1 = 2\sqrt{\frac{\varepsilon}{A}}U_1. \quad (4)$$

If the neutron and proton optical potentials at a given energy are well determined from the optical-model (OM) analysis of the corresponding elastic data, then the isovector term of the nucleon OP can be obtained directly from Eqs. (2) and (3) as

$$U_1 = \frac{(U_n - U_p)}{2\varepsilon}. \quad (5)$$

Unfortunately, isospin is not a good quantum number in the Coulomb field of the nucleus because this field slows the incident proton and affects the strength and shape of the proton-nucleus OP. It is necessary, therefore, to add Coulomb corrections ΔE_C to the incident proton energy and ΔU_C to U_p to separate the main effects of the Coulomb field so that isospin is a good quantum number for the remainder of the nucleon OP, namely,

$$U_p = U_0 - \varepsilon U_1 + \Delta U_C, \quad (6)$$

$$U_n = U_0 + \varepsilon U_1. \quad (7)$$

Then the Coulomb correction term must be determined from

$$\Delta U_C = U_p - U_n + 2\varepsilon U_1 \Longleftrightarrow U_1 - \frac{\Delta U_C}{2\varepsilon} = \frac{U_n - U_p}{2\varepsilon}. \quad (8)$$

In general, Eq. (8) has four unknowns (the real and imaginary parts of ΔU_C and U_1) that, as we will see, cannot be determined unambiguously even if the *complex* neutron and proton optical potentials are well determined.

There are "global" systematics of the OP parameters deduced from the extensive OM analyses of nucleon elastic scattering, for example, those by Becchetti and Greenlees [11], by Koning and Delaroche [12], and by Varner *et al.* [13]. In the work described here, we rely on the CH89 global model by Varner *et al.* The CH89 optical potentials cover a wide range of energies and target masses and are parametrized using Woods-Saxon (WS) forms. The resulting systematics are often used to predict the nucleon OP when elastic scattering data are not available or cannot be measured, as is the case for many unstable nuclei near the drip line. Given the large isospins of drip-line nuclei, it is important to estimate accurately the isospin dependence of the nucleon OP (or, equivalently, the Coulomb corrections to that OP) before applying it in studies of nuclear reactions or of astrophysical phenomena. So far, the empirical isospin dependence of the nucleon OP has been deduced [11–13] based mainly on the OM analyses of the proton and neutron elastic scattering, adopting some simple treatment of the Coulomb correction terms ΔE_C and ΔU_C.

Before the present measurement of neutron scattering on ^{208}Pb, detailed elastic $n + {}^{208}$Pb scattering data were available only at energies up to 26 MeV. This energy range, however, does not overlap that of much of the precise proton data and furthermore is too small to establish clearly the energy dependence of the neutron OP. The measurements at 30.4 and 40.0 MeV described here have greatly expanded the energy range for the neutron data and provided the most accurate and detailed data for neutron scattering above 26 MeV from any $N \neq Z$ nucleus. After our measurement, several experiments on the elastic $n + {}^{208}$Pb scattering were carried out and the neutron scattering data were measured at 65 MeV [14], in the forward angular region but over a wide range of the neutron incident energy from 65 to 225 MeV [15], and at the neutron energy of 96 MeV [16]. Together with the present data, one has now a good database of the elastic $n + {}^{208}$Pb scattering data to study the energy dependence of the neutron OP. In the present paper we show that the accurate neutron scattering data can also be used in a consistent analysis of the elastic neutron and proton scattering from ^{208}Pb and the charge-exchange $^{208}\mathrm{Pb}(p,n)^{208}\mathrm{Bi}^*_{\mathrm{IAS}}$ reaction to study the isovector part of the nucleon-nucleus OP, and to estimate the Coulomb correction term (8) to the proton OP.

II. EXPERIMENTAL METHOD

The measurements were performed using the Michigan State University beam swinger time-of-flight system [17–19] as modified for neutron scattering. Neutrons produced by the $^7\mathrm{Li}(p,n)^7\mathrm{Be}$(g.s. + 0.429 MeV) reaction scatter from a cylindrical 200.64-g target (2.40 cm diam × 3.90 cm long) of isotopically enriched ^{208}Pb (98.69%)[1] and are detected in a liquid scintillation counter with an overall time resolution of about 1.0 ns. This corresponds to an energy resolution for the elastic peak of better than 1.1 MeV FWHM, sufficient to resolve the first excited state of ^{208}Pb at 2.61 MeV. Pulse shape discrimination is used to eliminate the γ-ray background. The neutron detectors are situated in a room separated from the swinger vault by a 1.8-m-thick concrete wall, except for a hole to transmit the target scattered neutrons. Additional shielding against neutrons coming directly from the production reaction is provided by a movable 1.1-m-long iron shadow bar. A monitor time-of-flight detector is mounted rigidly to the beam swinger so as to measure neutron flux from the production reaction at a fixed angle near 22°. This monitor is used to

[1] ^{208}Pb target was obtained on loan from D. Drake, Los Alamos.

normalize the flux from run to run. Air scattering background is accounted for by measuring target-in and target-out spectra at each angle; a small correction is made to account for the fact that some of those air-scattered neutrons originating behind the sample are absorbed by the sample on their way to the detector [19]. Relative uncertainties are typically 2–4% but reach 8% at a few angles. Observation of the ^{7}Li(p,n) flux at 0° measures the product of incident neutron flux and detector efficiency and yields the absolute normalization to within 3%. Corrections are made for the dead time, source anisotropy, and background attenuation due to the sample. Further details of the experimental procedures can be found in Refs. [18,19].

III. DATA ANALYSIS AND DISCUSSION

A relatively large target was used to obtain adequate statistical accuracy, making it necessary to correct the experimental data for the effects of multiple scattering, angle averaging, and attenuation. Because the cross sections varied rapidly with angle we were concerned that the deconvolution procedures generally employed would lead to ambiguities and unacceptably large uncertainties. We elected to avoid these uncertainties by convoluting the results of optical-model predictions, a straightforward procedure, before comparing them with the data in a search routine. For this purpose, Kinney's finite geometry code [20] was incorporated as a subroutine of the optical model search code GIBELUMP [21]. The spin-orbit part of the neutron OP was fixed at that used in Ref. [22] for lower-energy neutron data, and the "average" geometry of the WS potential was taken from Ref. [23].

During the search, the smeared optical-model cross sections were compared with the experimental data and the optical-model parameters were adjusted until a good fit to the experimental data was obtained, thereby fixing the optical-model parameters. The cross sections and their uncertainties resulting from this procedure were then deduced. These cross sections are corrected for multiple scattering, angle averaging, and attenuation, and are shown in Fig. 1, Fig. 4, and Table I, respectively. The uncertainties resulting from the finite geometry corrections varied with angle and have

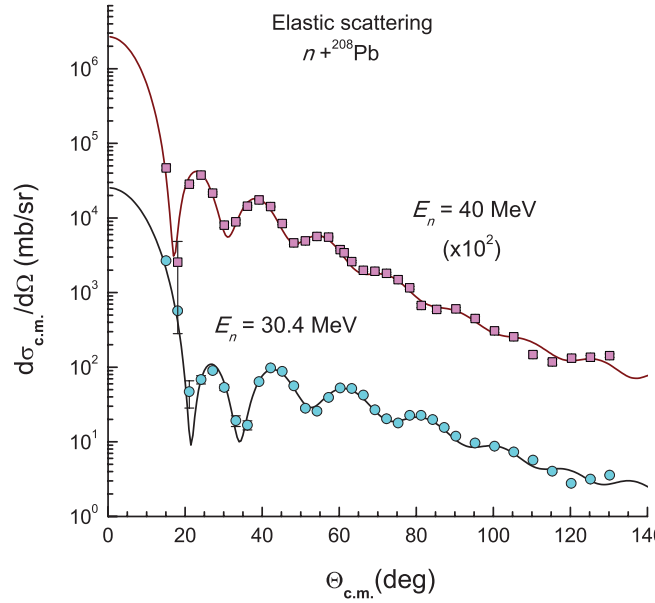

FIG. 1. (Color online) Elastic $n + ^{208}$Pb scattering data at 30.4 and 40 MeV, corrected for finite geometry effects as described in the text, are compared with the OM fit given by the modified CH89 optical potential (see OP parameters in Table II) and represent our best fit to the neutron data.

TABLE I. Measured cross sections of ^{208}Pb$(n,n)^{208}$Pb at 30.4 and 40 MeV. The cross sections are corrected for finite geometry effects as described in the text.

30.4 MeV						40.0 MeV					
$\theta_{c.m.}$ (deg)	$\sigma_{c.m.}$ (mb/sr)	$\Delta\sigma_{c.m.}$ (mb/sr)	$\theta_{c.m.}$ (deg)	$\sigma_{c.m.}$ (mb/sr)	$\Delta\sigma_{c.m.}$ (mb/sr)	$\theta_{c.m.}$ (deg)	$\sigma_{c.m.}$ (mb/sr)	$\Delta\sigma_{c.m.}$ (mb/sr)	$\theta_{c.m.}$ (deg)	$\sigma_{c.m.}$ (mb/sr)	$\Delta\sigma_{c.m.}$ (mb/sr)
15.07	2675	83.0	66.26	42.24	1.13	15.07	468.6	30.5	63.26	26.01	0.92
18.09	568.5	33.2	69.27	26.92	0.83	18.09	25.6	22.8	66.26	19.89	0.79
21.10	47.02	18.7	72.27	20.33	0.67	21.10	283.7	10.9	69.27	19.32	0.65
24.12	68.27	8.7	75.28	17.95	0.61	24.12	376.7	11.2	72.28	18.11	0.58
27.13	89.94	6.4	78.28	22.67	0.61	27.13	215.8	7.6	75.28	14.93	0.56
30.14	53.39	4.75	81.28	22.56	0.58	30.14	80.11	5.9	78.28	11.60	0.52
33.16	19.20	3.15	84.29	19.83	0.56	33.16	88.84	5.1	81.29	6.722	0.436
36.17	16.79	2.33	87.29	15.57	0.455	36.17	143.8	4.04	85.29	5.942	0.341
39.18	63.85	2.19	90.29	11.89	0.435	39.18	174.1	3.9	90.29	6.058	0.274
42.19	97.82	2.22	95.29	9.654	0.299	42.19	142.2	2.49	95.29	4.500	0.237
45.20	87.86	1.52	100.3	8.721	0.261	45.20	84.29	2.91	100.3	3.072	0.178
48.21	56.29	1.37	105.3	7.321	0.236	48.22	46.44	2.28	105.3	2.558	0.145
51.22	28.20	1.84	110.3	5.704	0.194	51.23	49.27	1.60	110.3	1.477	0.123
54.23	25.85	1.68	115.3	4.024	0.164	54.23	56.53	1.53	115.3	1.176	0.100
57.24	39.21	1.66	120.2	2.772	0.137	57.24	55.50	1.46	120.3	1.325	0.090
60.25	52.85	1.15	125.2	3.164	0.136	60.25	37.61	1.27	125.2	1.362	0.081
63.26	51.68	1.11	130.2	3.584	0.093	61.25	34.20	1.01	130.2	1.432	0.077

a maximum of about 8% at the first diffraction minimum. These uncertainties are included in the tabulated cross sections. Because this is an unconventional procedure its results were compared with the normal deconvolution procedure used at lower energies for the case of Fe at 26 MeV; the two procedures yielded close agreement. The analysis process is described in much more detail in Refs. [18,19].

The deduced center-of-mass (c.m.) cross sections [18] of the elastic $n + {}^{208}$Pb scattering at 30.4 and 40 MeV have been studied in several OM analyses, including extensive searches for global parameters of the nucleon OP [12]. In the present work, a detailed OM analysis of the measured elastic $n + {}^{208}$Pb scattering data was made using the CH89 geometric parameters of the nucleon OP [13]. The OM analysis and coupled-channel calculation of the (p,n) reaction were made using the code ECIS97 written by Raynal [24].

A. Coulomb correction to the proton incident energy

The Coulomb correction to the proton incident energy arises because the proton slows down in the repulsive Coulomb field of the nucleus and, hence (because the real part of the OP decreases with increasing energy), the real part of U_p is more attractive compared to that of the neutron OP at the same bombarding energy, even when $U_1 = 0$. Estimation of the Coulomb correction of the nucleon OP requires that one first determine the difference in the effective proton and neutron incident energies, so that the same isoscalar and isovector potentials $U_{0(1)}$ can be used to generate the proton and neutron OPs using Eq. (2).

The difference in the proton and neutron energies has usually been assumed either to be constant at the average Coulomb energy of the incident proton, $\Delta E_C = 6Ze^2/(5R_C) \approx 19$ MeV for a ^{208}Pb target [13], or to be energy dependent [12]. In the present work we chose the CH89 global parametrization for the nucleon OP, which has a simple functional form and is quite reliable for the nucleon elastic scattering from medium-mass nuclei at energies of 10 to 65 MeV, as the starting point of our OM analysis. The CH89 complex nucleon OP is determined as the following energy-dependent functional:

$$U(E) = U_0(E - \Delta E_C) \mp \varepsilon U_1(E - \Delta E_C), \qquad (9)$$

with $-$ and $+$ sign pertaining to the incident proton and neutron, respectively. Thus, the CH89 proton and neutron optical potentials determined at energies E_p and $E_n = E_p - \Delta E_C$, respectively, should be fully consistent with the Lane formalism in Eqs. (2) and (3). We discuss below the extent to which this assumption accurately describes the experimental data.

To obtain an estimate of ΔE_C based on experiment, we determined the proton bombarding energy at which the slowed proton and the neutron have the same average momentum, and thereby the diffraction maxima and minima of the proton and neutron angular distributions fall at about the same (average) angles in the forward region [25]. For this purpose, the diffractive oscillation of the elastic $n + {}^{208}$Pb data at 30.4 MeV was compared with those of the elastic $p + {}^{208}$Pb scattering at 45, 47.3, and 49.4 MeV (see Fig. 2). It is clear that the

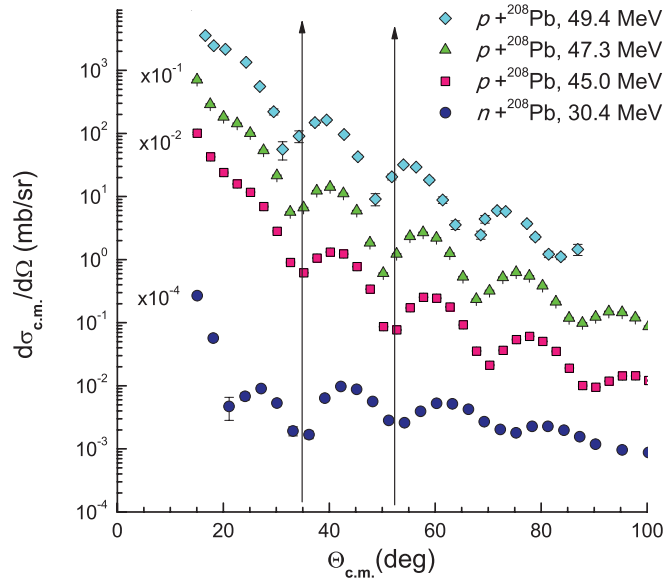

FIG. 2. (Color online) Diffractive oscillation of the elastic $n + {}^{208}$Pb scattering data at 30.4 MeV in comparison with those of elastic $p + {}^{208}$Pb scattering data at 45, 47.3 [23], and 49.4 MeV [26].

oscillation pattern of the 30.4-MeV neutron data does not agree with that of the 49-MeV proton data, as would be expected from the average Coulomb energy prescription of the CH89 model. The elastic $p + {}^{208}$Pb scattering data at 45 MeV [23] do have an oscillation pattern at forward angles very similar to that of the 30.4-MeV neutron data. This implies that $\Delta E_C \approx 14.6$ MeV, significantly smaller than the value of 19 MeV used in the CH89 parametrization.

Our procedure presumably equalizes the average momenta or wavelengths of the neutrons and protons in the regions dominating the scattering. For illustration, we plot in Fig. 3 the local nucleon (relative motion) momentum $K(R)$ determined

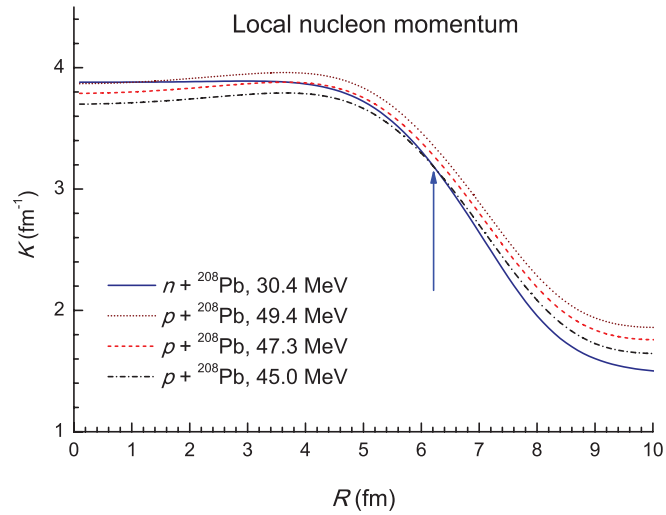

FIG. 3. (Color online) Local nucleon momentum $K(R)$ determined from Eq. (10) with the real OP given by the folding calculation [7,9], using the density-dependent CDM3Y6 interaction [27].

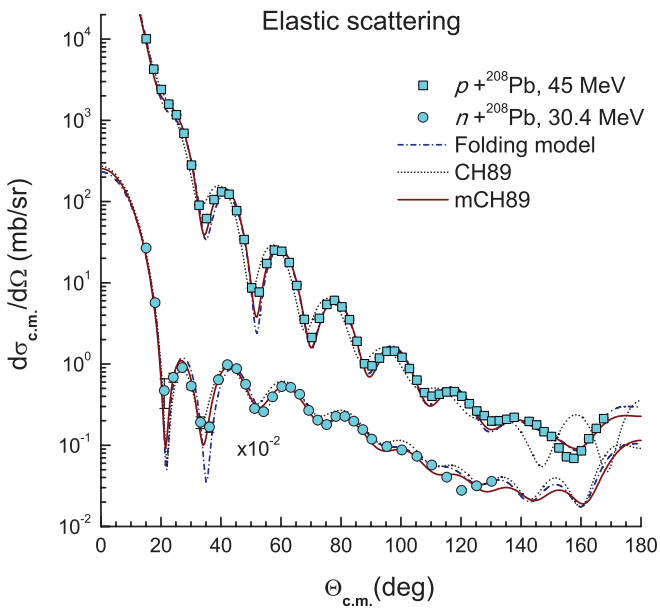

FIG. 4. (Color online) OM description of the elastic $n + {}^{208}$Pb data at 30.4 MeV and $p + {}^{208}$Pb data at 45 MeV [23] given by the CH89 (dotted line), mCH89 (solid line), and the folded (dash-dotted line) optical potentials.

from the real folded nucleon OP [7] as

$$K^2(E, R) = \frac{2\mu}{\hbar^2}[E_{\text{c.m.}} - V(R) - V_C(R)], \tag{10}$$

where μ is the nucleon reduced mass, and $V(R)$ and $V_C(R)$ are, respectively, the real central nuclear and Coulomb parts of the OP ($V_C \equiv 0$ for the neutron-nucleus system). It can be seen from Fig. 3 that the local momentum of 30-MeV neutrons is equal that of 45-MeV protons at $R \sim 6$ fm, in the surface region of the ^{208}Pb target. Because the diffractive scattering is dominantly determined by the strength and shape of the OP at the surface, the results plotted in Fig. 3 support a Coulomb correction of $\Delta E_C \approx 14.6$ MeV at a proton incident energy of 45 MeV.

Finally, in Fig. 4 we show OM calculations with several related optical potentials to assess differences in the cross sections they predict. First, the two data sets were compared with calculations using the original CH89 parameters [13], but with ΔE_C set to 14.6 MeV at 45 MeV proton energy. Then the potential depths were adjusted, yielding mCH89 OP, to give the best χ^2 fit to the data. For a comparison, OM results given by the complex folded potential [9] calculated with the CDM3Y6 interaction [27] (strengths of the real and imaginary folded potentials were adjusted to the best χ^2 fit to the data) are shown.

B. ^{208}Pb$(p,n)^{208}$Bi$^*_{\text{IAS}}$ data and the isovector term of the OP

In the two-channel approximation for the charge-exchange (p,n) reaction exciting IAS, the total wave function can be written as

$$\Psi = |pA\rangle\chi_{pA}(\boldsymbol{R}) + |n\tilde{A}\rangle\chi_{n\tilde{A}}(\boldsymbol{R}), \tag{11}$$

where the $\chi(\boldsymbol{R})$ describe the relative nucleon-nucleus motion. The elastic (p,p) scattering and charge-exchange $A(p,n)\tilde{A}_{\text{IAS}}$ cross sections are then obtained from the solutions of the following coupled-channel (CC) equations [3]:

$$[K_p + U_p(R) - E_p]\chi_{pA}(\boldsymbol{R}) = -F_{pn}(R)\chi_{n\tilde{A}}(\boldsymbol{R}), \tag{12}$$

$$[K_n + U_n(R) - E_n]\chi_{n\tilde{A}}(\boldsymbol{R}) = -F_{pn}(R)\chi_{pA}(\boldsymbol{R}). \tag{13}$$

Here $K_{p(n)}$ and $E_{p(n)}$ are the kinetic-energy operators and c.m. energies of the $p + A$ and $n + \tilde{A}$ partitions. The proton OP in the entrance $(p + A)$ channel was determined from the best OM fit to the elastic $p + {}^{208}$Pb scattering data at 45 MeV (see Fig. 4 and potential parameters in Table II), while the neutron OP in the outgoing $(n + \tilde{A})$ channel was constructed from the isoscalar and isovector parts of the nucleon OP using the standard isospin coupling scheme [3,9]. Because the energies of isobar analog states are separated approximately by the Coulomb displacement energy, the (p,n) transition between them has a nonzero Q value. To account for this effect, the isoscalar U_0 and isovector U_1 potentials used to construct $F_{pn}(R)$ and $U_n(R)$ were evaluated from the CH89 systematics at an effective incident energy of $E = E_{\text{lab}} - Q/2$, midway between the energies of the incident proton and emergent neutron [2]. Given the elastic $p + {}^{208}$Pb scattering data [23] and charge-exchange ^{208}Pb$(p,n)^{208}$Bi$^*_{\text{IAS}}$ data [28] (both measured at 45 MeV), we were able to test the isovector term U_1 of the proton OP by comparing the results of the CC calculation for the (p,n) cross section with the data. One can see in Fig. 5 that the isovector part of the CH89 nucleon OP [13] accounts very well for the (p,n) data, especially when the WS strengths of the proton OP are optimized by the best χ^2 fit to the elastic (p,p) data at 45 MeV (the mCH89 potential in Table II). This result shows that the complex isovector potential U_1 given by the CH89 parametrization for the proton OP at 45 MeV can be used to estimate the Coulomb correction using Eq. (8) and the corresponding neutron optical potential U_n.

C. Coulomb correction to the proton OP

After ΔE_C has been fixed to give the same diffraction patterns at the forward angles for the proton and neutron elastic cross sections at E_p and $E_n = E_p - \Delta E_C$, respectively, one might naively expect from Eq. (9) that the corresponding proton and neutron optical potentials are fully Lane consistent. But this is only true if the only physics involved is that due to the energy shift. Yet we know there are other effects, mostly affecting the imaginary potential, for example, Coulomb excitation, different Q values for (p,n) and (n,p) reactions, and different level structures. In the following we obtain an estimate of the importance of such phenomena.

Given that the isovector potential U_1 of the CH89 potential was shown above to give a realistic description of the (p,n) data, it is reasonable to use U_1 given by the CH89 systematics to estimate ΔU_C, based on the OM analysis of the elastic $p + {}^{208}$Pb and $n + {}^{208}$Pb scattering data measured at 45 and 30.4 MeV. In our OM analysis we used the same WS functional form for the nucleon OP as that used by the CH89 systematics [13], so the real and imaginary parts of the nucleon OP are

TABLE II. OP parameters (14) and (15) used in the OM analysis of the elastic $p + {}^{208}$Pb data and $n + {}^{208}$Pb data. The radii and diffuseness parameters were given by the CH89 parametrization (in fm): $R_v = 7.18$, $R_w = 7.46$, $a_v = a_w = 0.69$, $R_{so} = 6.73$, $a_{so} = 0.63$. The incident energy E, Coulomb corrections (17) and (18), and potential depths are given in MeV. The real strength of the isovector potential was taken as $\varepsilon V_1 = 2.77 \pm 0.17$ MeV; its imaginary strength εW_1 and the Coulomb correction strengths ΔV_v, ΔW_v, and ΔW_s are given with uncertainties (in brackets) estimated from those of our OM fit and the CH89 potential parameters [13].

System	E	Potential	V_v	ΔV_v	W_v	ΔW_v	W_s	ΔW_s	εW_1	V_{so}
$p + {}^{208}$Pb	54.2	CH89	43.71	0.00	4.50	0.00	6.53	0.00	−1.80 (0.11)	5.90
		mCH89	40.61	−1.90 (0.56)	4.67	−0.20 (0.30)	5.03	−1.88 (0.51)	−1.80 (0.11)	5.90
$n + {}^{208}$Pb	40.0	CH89	38.17		4.50		2.93		1.80 (0.11)	5.90
		mCH89	36.97		4.87		3.31		1.80 (0.11)	6.11
$p + {}^{208}$Pb	45.0	CH89	46.58	0.00	3.34	0.00	7.43	0.00	−2.05 (0.13)	5.90
		mCH89	43.27	−1.94 (0.54)	3.69	−0.75 (0.26)	5.72	−1.18 (0.52)	−2.05 (0.13)	4.22
$n + {}^{208}$Pb	30.4	CH89	41.04		3.34		3.33		2.05 (0.13)	5.90
		mCH89	39.67		4.44		2.80		2.05 (0.13)	6.47

determined as

$$V(R) = -V_v f_{WS}(R, R_v, a_v) + \frac{2V_{so}}{R}\frac{d}{dR} f_{WS}(R, R_{so}, a_{so})(\boldsymbol{l}\cdot\boldsymbol{\sigma}), \quad (14)$$

$$W(R) = -W_v f_{WS}(R, R_w, a_w) + 4a_w W_s \frac{d}{dR} f_{WS}(R, R_w, a_w),$$

$$\text{where} \quad f_{WS}(R, R_x, a_x) = 1/\{1 + \exp[(R - R_x)/a_x]\}. \quad (15)$$

The real part of the proton OP includes the Coulomb potential $V_C(R)$ taken from the CH89 systematics [13]. The CH89 parametrization gives the isovector part U_1 of the nucleon OP as

$$U_1(R) = V_1 f_{WS}(R, R_v, a_v) - i4a_w W_1 \frac{d}{dR} f_{WS}(R, R_w, a_w). \quad (16)$$

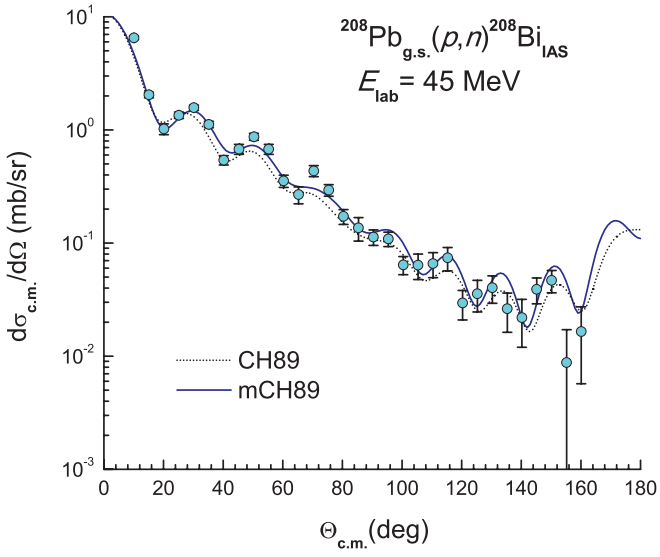

FIG. 5. (Color online) Coupled-channel description of the charge-exchange ^{208}Pb$(p,n)^{208}$Bi$^*_{IAS}$ data measured at 45 MeV [28] given by F_{pn} built upon the isovector part U_1 of the CH89 nucleon OP [13]. The two different curves were obtained with two choices of the 45 MeV proton OP (see Table II).

For the proton OP at 45 MeV, the complex strength of the isovector potential is readily obtained from the CH89 parametrization as $\varepsilon V_1 = 2.77 \pm 0.17$ MeV and $\varepsilon W_1 = 2.05 \pm 0.13$ MeV. The quoted uncertainties were determined from the systematic uncertainties of the CH89 global parameters [13].

In the present OM analysis, we first generated the complex $p + {}^{208}$Pb and $n + {}^{208}$Pb optical potentials using the CH89 parametrization but with a corrected $\Delta E_C = 14.6$ MeV for the proton OP (see CH89 parameters in Table II). As a result, the CH89 optical potentials for 45 MeV proton and 30.4 MeV neutron are *fully Lane consistent*, with the Coulomb correction taken into account only by using the energy shift ΔE_C in Eq. (9), and its remnant, determined by Eqs. (17) and (18), is exactly zero. The OM description of the 30 MeV neutron and 45 MeV proton elastic scattering by the Lane-consistent CH89 optical potentials is shown in Fig. 4 as dotted lines. One can see that the Lane-consistent CH89 OP describes the data fairly well, excepting at the backward angles where it fails to follow the oscillation pattern of the measured (p,p) data. A much-improved OM description of the data has been achieved by adjusting the depths of the OP while keeping the same WS geometry as that of the CH89 potential (see mCH89 parameters in Table II and solid lines in Fig. 4). Such an adjustment procedure naturally gave rise to a nonzero remnant of the Coulomb correction $\Delta U_C = \Delta V_C + i\Delta W_C$. Assuming the same U_1 for the mCH89 OP as that of the original CH89 OP, the *complex* remnant of the Coulomb correction can be explicitly determined from Eqs. (8), (14), and (15) as

$$\Delta V_C(R) = -\Delta V_v f_{WS}(R, R_v, a_v), \quad (17)$$

$$\Delta W_C(R) = -\Delta W_v f_{WS}(R, R_w, a_w) + 4a_w \Delta W_s \frac{d}{dR} f_{WS}(R, R_w, a_w). \quad (18)$$

The deduced WS strengths (18) of ΔU_C, further referred to as the Coulomb correction to the mCH89 proton OP, are given in Table II with the uncertainties estimated consistently from the standard errors of the OM fits and those of the CH89 potential parameters. Although the strengths of the spin-orbit potential V_{so} of the best-fit mCH89 optical potentials also differ from

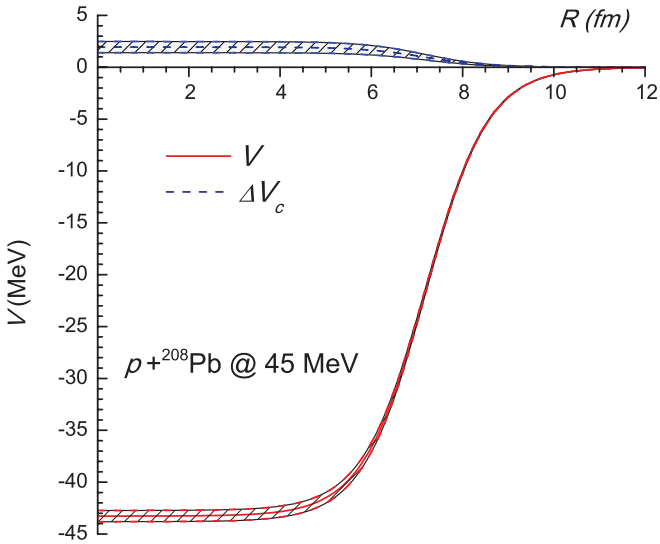

FIG. 6. (Color online) Real central OP of 45-MeV protons and the corresponding Coulomb correction ΔV_C determined from Eq. (17) using the mCH89 optical potentials for 30-MeV neutrons and 45-MeV protons. The uncertainties were estimated from that given by the CH89 systematics for $\varepsilon\Delta V_1$ and standard errors of the OM fit with the code ECIS97 [24].

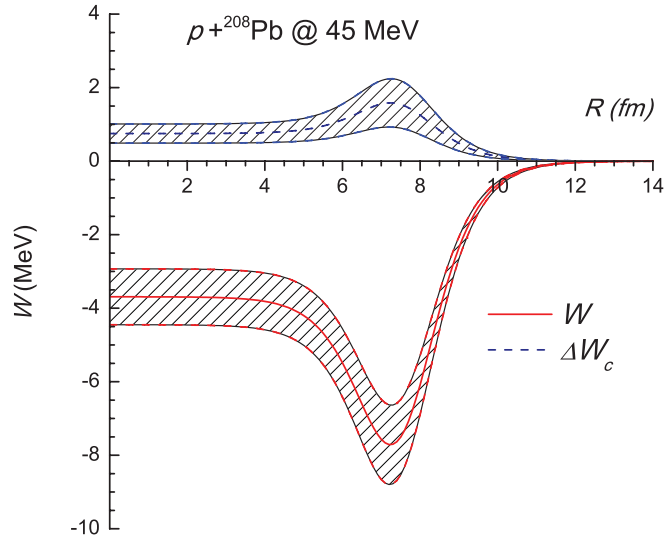

FIG. 7. (Color online) The same as Fig. 6 but for the imaginary part of the central OP, with the corresponding Coulomb correction ΔW_C determined from Eq. (18).

the original CH89 values, we did not assign this difference to the isospin impurity of the OP caused by the Coulomb correction.

From the strengths of the Coulomb correction ΔU_C to the best-fit mCH89 optical potentials for the elastic neutron and proton scattering at 30.4 and 45 MeV, respectively, we find the following ratios of the Coulomb correction to the strength of the OP: $\Delta V_v/V_v \approx 4.5\%$, $\Delta W_v/W_v \approx 20.3\%$, and $\Delta W_s/W_s \approx 20.6\%$. It is obvious that, within the Lane formalism (1), these ratios give us a realistic estimate of the *isospin impurity* of the mCH89 nucleon OP. The radial dependence of the Coulomb correction to the real and imaginary parts of the central OP is plotted in Figs. 6 and 7, respectively, where one can see clearly a repulsive character of the Coulomb correction to both the real and imaginary OP. In terms of the isospin impurity, we conclude that the Lane formulation (1) is accurate to within about 4–5% for the real central OP. However, the isospin impurity becomes much larger (above 20%) for the imaginary part of the CH89 OP and reaches its peak at the surface.

In a study of the elastic $n + {}^{208}$Pb scattering at 40 MeV similar to that described above for 30.4-MeV neutrons, and using the complex CH89 OP [13] to predict the elastic $p + {}^{208}$Pb scattering at the higher energies, we find that the elastic proton scattering at 54.2 MeV has about the same forward angle diffraction pattern as the measured elastic $n + {}^{208}$Pb scattering at 40 MeV, yielding $\Delta E_C \approx 14.2$ MeV for the 54-MeV proton potential. There are no elastic proton data available near 54 MeV, so we compare in Fig. 8 only the OM prediction for the elastic $p + {}^{208}$Pb scattering at 54.2 MeV with the elastic $n + {}^{208}$Pb data at 40 MeV. To roughly estimate the Coulomb correction for 54.2-MeV protons we have scaled the real and imaginary WS strengths of the CH89 OP by the same factors deduced from the corresponding strengths of the mCH89 OP compared to those of the CH89 OP for 45-MeV protons. The parameters obtained are given in Table II as mCH89. We note that the imaginary parts of the CH89 and mCH89 proton OPs at 54.2 MeV give total reaction cross sections $\sigma_R \approx 2121$ and 2050 mb, respectively, and that the latter value agrees quite well with the experimental trend: measured values of σ_R lie around 2000 mb at proton energies of 40 to 60 MeV [29]. We have further assumed the same U_1

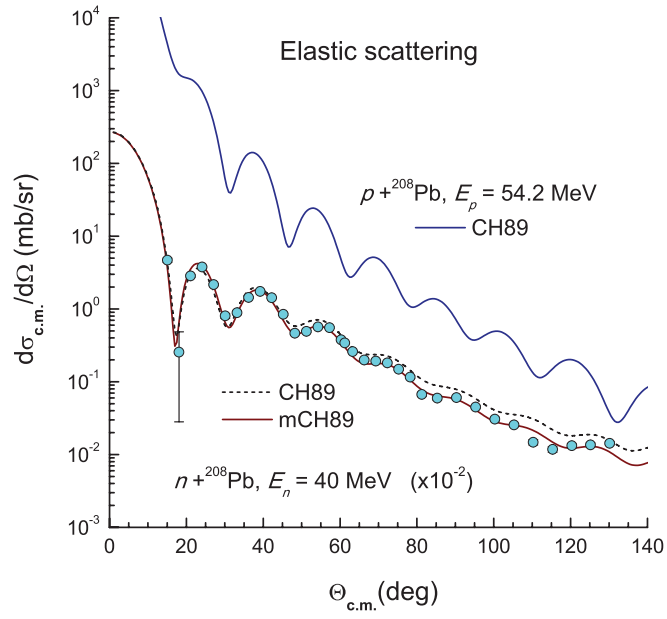

FIG. 8. (Color online) OM description of the elastic $n + {}^{208}$Pb data at 40 MeV given by the CH89 OP (dashed line) and mCH89 OP (solid line). The OM prediction for the elastic $p + {}^{208}$Pb scattering at 54.2 MeV is given by the CH89 OP, with the Coulomb correction to the proton incident energy $\Delta E_C \approx 14.2$ MeV.

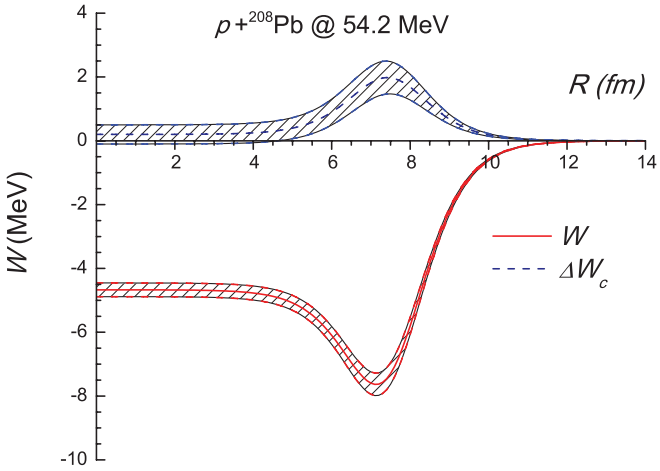

FIG. 9. (Color online) The same as Fig. 7 but for the imaginary part of the mCH89 optical potential of the 54.2-MeV proton (see Table II).

for the mCH89 proton OP at 54.2 MeV as that given by the original CH89 parameters for 54.2 MeV protons and deduced the Coulomb correction ΔU_C to the mCH89 proton OP in the same way as done above for 45 MeV protons. We find a behavior of ΔU_C very similar to that found for 45-MeV protons, with a rather strong ΔW_C peaked at the nuclear surface (see Fig. 9).

IV. DISCUSSION

We find that $p + {}^{208}$Pb data at proton incident energies of 45 and 54.2 MeV have close to the same diffraction pattern as elastic neutron scattering at 30.4 and 40 MeV, corresponding to energy shifts ΔE_C of 14.6 and 14.2, respectively, owing to Coulomb repulsion effects. Using $E_p = E_n + \Delta E_C$ (with the Coulomb correction taken into account by the CH89 systematics), we found that the best-fit proton OP still contains a nonzero remnant of the Coulomb correction, which represents the isospin impurity of the nucleon OP. While the correction to the real part of the proton OP is only a few percent, as might be expected from the mean-field nature of the *real* nucleon OP, the correction to the imaginary part at the nuclear surface is about 20%.

Such a significant isospin impurity of the imaginary OP found in our analysis also confirms the trend found recently in a global dispersive optical model (DOM) analysis of elastic proton and neutron scattering [30]. Namely, from a comparison of the elastic proton and neutron data on ^{208}Pb, the surface component of the imaginary OP obtained in the DOM has shown quite different $(N\text{-}Z)$ asymmetry dependencies between protons and neutrons. Such a difference results directly in a deviation of the isospin dependence of the nucleon OP from the Lane form of Eqs. (2) and (3) and gives rise, therefore, to a larger Coulomb correction to imaginary OP at the nuclear surface.

These differences indicate that there are different mechanisms for proton and neutron absorption that are linked to different nonelastic reaction channels induced by protons and neutrons on a ^{208}Pb target. The most obvious of these are Coulomb excitation and a difference in the Q values of the (n,p) and (p,n) reactions. Because the physics origin of the imaginary OP is multifaceted and contains dynamic higher-order (beyond the mean field) contributions, the significant isospin impurity found for the imaginary part of the nucleon OP was not unexpected. One needs an explicit microscopic calculation of the imaginary OP based, e.g., on the Feshbach formalism [31] to establish full Lane consistency of the mean-field part of the nucleon OP. The present results are also in a qualitative agreement with the Brueckner-Hartree-Fock calculation of the nucleon OP by Jeukenne *et al.* [6], which showed that for heavy nuclei such as ^{208}Pb the imaginary Coulomb correction can be quite significant.

Our results show that some treatments of the Coulomb correction adopted in the literature are probably inadequate. For example, the CH89 systematics [13] uses the same energy shift ΔE_C for the real and imaginary OP and it underestimates, therefore, the Coulomb correction to the imaginary OP as shown above. The recent global OP by Koning and Delaroche [12] even assumes $\Delta W_C \approx 0$.

We note that another common usage for Coulomb correction is the entire difference of the OP for neutrons and protons at the same energy. To show the strength of such a total Coulomb correction, we generated the 45-MeV proton OP using the same CH89 formulas but setting $\Delta E_C = 0$. This procedure yields a significantly stronger ΔU_C, with $\Delta V_v/V_v \approx 5.6\%$, $\Delta W_v/W_v \approx 56.9\%$, and $\Delta W_s/W_s \approx 12.9\%$. However, one should be careful in discussing such a total Coulomb correction because the CH89 formulas were determined [13] using a constant energy shift $\Delta E_C = 19$ MeV for $p + {}^{208}$Pb OP, and it is questionable to use the CH89 potential obtained with $\Delta E_C = 0$ in the present discussion.

V. SUMMARY

We measured cross sections for elastic scattering of neutrons from ^{208}Pb at 30.4 and 40.0 MeV and deduced the realistic OP parameters using the Woods-Saxon geometry given by the CH89 systematics.

The elastic $p + {}^{208}$Pb scattering data at 45 MeV and elastic $n + {}^{208}$Pb scattering data at 30.4 MeV have about the same diffractive structure at the forward angles, indicating that the energy shift used for 45-MeV protons in the CH89 parametrization should be $\Delta E_C \approx 14.6$ MeV. The isovector part U_1 of the nucleon OP for a ^{208}Pb target was used in a CC analysis of the charge-exchange (p,n) reaction at 45 MeV, exciting the IAS in ^{208}Bi, and a very satisfactory description of the (p,n) data was obtained. This result allowed us to use the complex isovector part U_1 of the CH89 OP to check the Lane consistency of the nucleon OP.

The detailed OM analysis of the elastic neutron and proton scattering has shown that the realistic proton OP at energy $E_p = E_n + \Delta E_C$ contains a nonzero Coulomb correction to its complex strength. Such a nonzero Coulomb correction represents the isospin impurity of the CH89 nucleon OP, which is only a few percent for the real part of the OP but is around 20% for the imaginary part at the nuclear surface.

We reiterate that these comments are in reference to the CH89 global OP, which already contains a significant correction for Coulomb effects. These results show that CH89 systematics provides an accurate estimate of Coulomb effects for the real part of the OP, provided that the energy shifts that enter the model are found by matching diffraction structures for neutron and proton scattering. The 20% correction for the imaginary part of the OP is not large, and the CH89 systematics can still provide a reasonable *a priori* estimate even for the imaginary potential.

These results confirm again the importance of elastic neutron-scattering experiments, for use in conjunction with existing elastic proton-scattering and (p,n) charge-exchange data, to obtain estimates of Coulomb corrections in heavy nuclei.

ACKNOWLEDGMENTS

We wish to thank Darrell Drake for the loan of the ^{208}Pb target. This research was supported by the US National Science Foundation Grants No. PHY-78-22696, No. PHY06-06007, and No. PHY08-22648(JINA). Two of the authors (D.T.K. and B.M.L.) were supported by the National Foundation for Science and Technology Development (NAFOSTED) under Project No. 103.04-2011.21.

[1] A. M. Lane, Phys. Rev. Lett. **8**, 171 (1962); Nucl. Phys. **35**, 676 (1962).
[2] G. R. Satchler, R. M. Drisko, and R. H. Bassel, Phys. Rev. **136**, B637 (1964).
[3] G. R. Satchler, *Direct Nuclear Reactions* (Clarendon Press, Oxford, 1983).
[4] J. Rapaport, V. Kulkarni, and R. W. Finlay, Nucl. Phys. A **330**, 15 (1979); G. R. Satchler, in *Isospin in Nuclear Physics*, edited by D. J. Wilkinson (North-Holland, Amsterdam, 1969), p. 389.
[5] D. M. Patterson, R. R. Doering, and A. Galonsky, Nucl. Phys. A **263**, 261 (1976).
[6] J. P. Jeukenne, A. Lejeune, and C. Mahaux, Phys. Rev. C **15**, 10 (1977).
[7] D. T. Khoa, E. Khan, G. Colò, and N. Van Giai, Nucl. Phys. A **706**, 61 (2002).
[8] D. T. Khoa, Phys. Rev. C **68**, 011601(R) (2003).
[9] D. T. Khoa, H. S. Than, and D. C. Cuong, Phys. Rev. C **76**, 014603 (2007).
[10] P. D. Kunz, in *The (p, n) Reaction and the Nucleon-Nucleon Force*, edited by C. D. Goodman, S. M. Austin, S. D. Bloom, J. Rapaport, and G. R. Satchler (Plenum Press, New York, 1980).
[11] F. D. Becheetti and G. W. Greenlees, Phys. Rev. **182**, 1190 (1969).
[12] A. J. Koning and J. P. Delaroche, Nucl. Phys. A **713**, 231 (2003).
[13] R. L. Varner, W. J. Thompson, T. L. McAbee, E. J. Ludwig, and T. B. Clegg, Phys. Rep. **201**, 57 (1991).
[14] E. L. Hjort, F. P. Brady, J. L. Romero, J. R. Drummond, D. S. Sorenson, J. H. Osborne, B. McEachern, and L. F. Hansen, Phys. Rev. C **50**, 275 (1994).
[15] J. H. Osborne, F. P. Brady, J. L. Romero, J. L. Ullmann, D. S. Sorenson, A. Ling, N. S. P. King, R. C. Haight, J. Rapaport, R. W. Finlay, E. Bauge, J. P. Delaroche, and A. J. Koning, Phys. Rev. C **70**, 054613 (2004).
[16] J. Klug *et al.*, Phys. Rev. C **67**, 031601(R) (2003); A. Öhrn *et al.*, *ibid.* **77**, 024605 (2008).
[17] R. K. Bhowmik, R. R. Doering, L. E. Young, S. M. Austin, A. Galonsky, and S. D. Schery, Nucl. Instrum. Methods **143**, 63 (1977).
[18] R. P. DeVito, Ph.D. thesis, Michigan State University, 1979 (unpublished).
[19] R. P. DeVito, S. M. Austin, U. E. P. Berg, W. Sterrenburg, and L. E. Young, Nucl. Instrum. Methods **215**, 423 (1983).
[20] W. E. Kinney, Nucl. Instrum. Methods **83**, 15 (1970).
[21] GIBELUMP was written by F. G. Perey and modified by R. M. Haybron. See also Ref. [19].
[22] J. Rapaport, T. S. Cheema, D. E. Bainum, R. W. Finlay, and J. D. Carlson, Nucl. Phys. A **296**, 95 (1978).
[23] W. T. H. van Oers, Huang Haw, N. E. Davison, A. Ingemarsson, B. Fagerström, and G. Tibell, Phys. Rev. C **10**, 307 (1974).
[24] J. Raynal, *Computing as a Language of Physics* (IAEA, Vienna, 1972), p. 75; coupled-channel code ECIS97 (unpublished).
[25] R. P. DeVito, S. M. Austin, W. Sterrenburg, and U. E. P. Berg, Phys. Rev. Lett. **47**, 628 (1981)
[26] G. S. Mani, D. T. Jones, and D. Jacques, Nucl. Phys. A **165**, 384 (1971).
[27] D. T. Khoa, G. R. Satchler, and W. von Oertzen, Phys. Rev. C **56**, 954 (1997).
[28] R. R. Doering, D. M. Patterson, and A. Galonsky, Phys. Rev. C **12**, 378 (1975).
[29] R. F. Carlson, At. Data Nucl. Data Tables **63**, 93 (1996).
[30] J. M. Mueller, R. J. Charity, R. Shane, L. G. Sobotka, S. J. Waldecker, W. H. Dickhoff, A. S. Crowell, J. H. Esterline, B. Fallin, C. R. Howell, C. Westerfeldt, M. Youngs, B. J. Crowe, and R. S. Pedroni, Phys. Rev. C **83**, 064605 (2011).
[31] H. Feshbach, *Theoretical Nuclear Physics* (Wiley, New York, 1992), Vol. II.